Hardware-Adapted Quantum Machine Learning: Supplementary materials

Ignacio Benito Acedo Blanco[†]
Carlos Ruíz Pastor
Javier González Conde

This supplementary document provides additional details and analyses to complement the master's thesis. It includes extended numerical results, supplementary figures and tables, and any additional data that support the findings presented.
Specifically, this document is organized as follows: in Section 1 we introduce new datasets to perform more experiments, in Section 2 we depict the encoding step for every dataset, Section 3 studies the predictions heatmaps and runs the main numerical results for the These materials are intended to provide all necessary information to fully understand and validate the study's conclusions.

1 Datasets

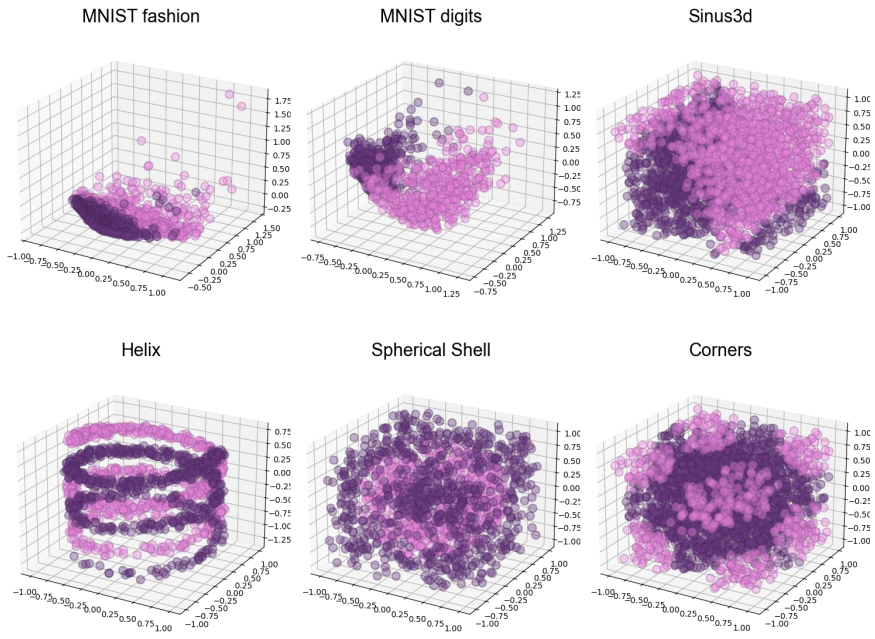

Figure 1: Datasets used for classification. MNIST datasets are reduced to three-dimensional points using classical PCA techniques.

We focus on the same four datasets described in the numerical results section and introduce two additional synthetic datasets: the helix and sinus datasets. These synthetic datasets, inspired by the original model article [1], were specifically designed to highlight the capabilities and limitations of the proposed quantum machine learning model. All datasets are visualized in Fig. 1. The MNIST datasets, originally consisting of images, are preprocessed using classical Principal Component Analysis (PCA) to reduce their dimensionality to three, facilitating their use with the newly designed Pulsed Quantum Machine Learning (PQML) model.
In this document, we not only present the simulation results for classification accuracy with the novel model but also analyze in detail the encoding strategies and decision boundary construction. Since proper three-dimensional

[†]100511795@alumnos.uc3m.es

visualizations of the decision boundaries are impractical, two-dimensional versions of the datasets have been created for illustrative purposes. For the synthetic datasets, this was achieved by direct dimensionality reduction, while for the MNIST datasets, classical PCA was applied. These two-dimensional representations are shown in Fig. 2. Note that the two-dimensional datasets used in this analysis are identical to those proposed in the original model

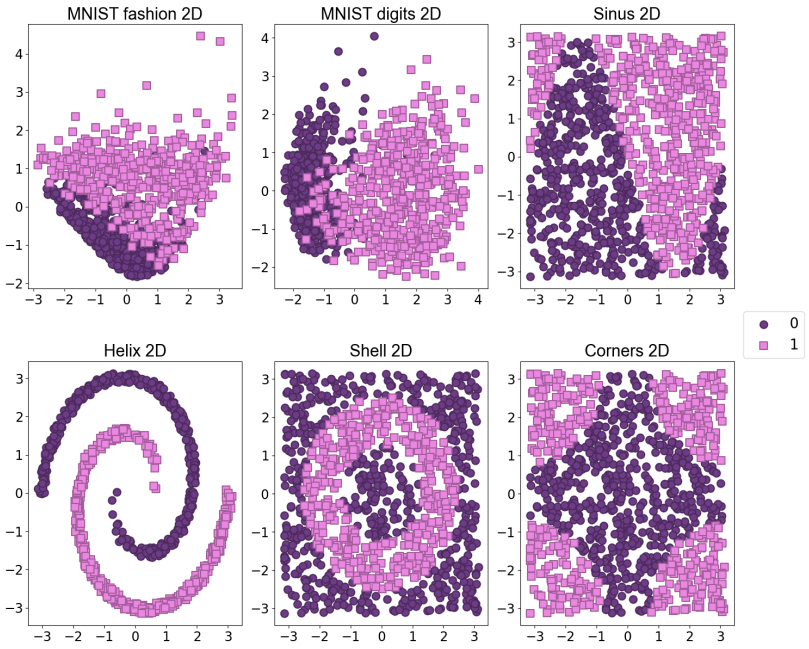

Figure 2: Two-dimensional version of the different datasets.

2 Encoding

In this section, we analyze the encoding step applied to each dataset, as illustrated in Figs. 3 and 4.
Datasets with some degree of spherical symmetry are particularly well-suited for the new pulse-based encoding, as demonstrated by the *spherical shell* and *corners* datasets. In these cases, the inherent structure of the data aligns naturally with the spherical coordinates used in the encoding, enabling clear separation between classes. This highlights the potential of the pulse-based approach for datasets that exhibit geometric properties conducive to spherical representations, where the encoding can fully leverage its ability to preserve the data's structure while simplifying decision boundaries.

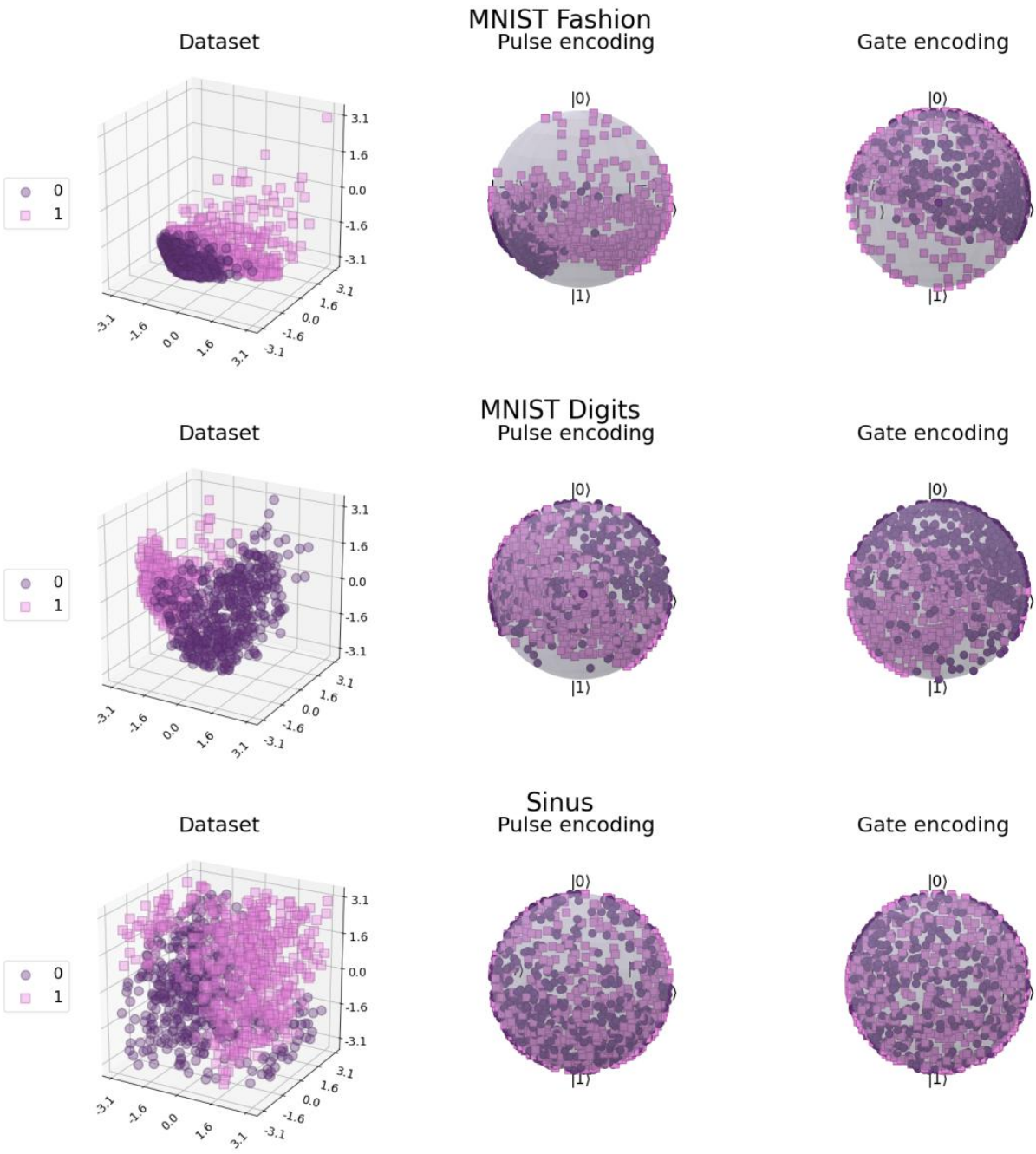

Figure 3: One step encoding applied to **fashion, digits and sinus** datasets for the gate-baesd and pulse-based strategies.

Conversely, the limitations of the pulse-based encoding become apparent with the *helix* dataset. Here, the dataset's complex, intertwined structure makes it inherently challenging to distinguish between classes using spherical coordinates. The continuous twisting nature of the data cannot be effectively captured within the constraints of the pulse-based encoding. In this scenario, the gate-based encoding demonstrates its strengths. While it may not preserve geometric structures as effectively as the pulse-based method, its greater expressiveness and adaptability enable it to better capture complex class distinctions. This adaptability makes the gate-based approach more suitable for datasets that lack symmetry or exhibit non-trivial structural patterns.

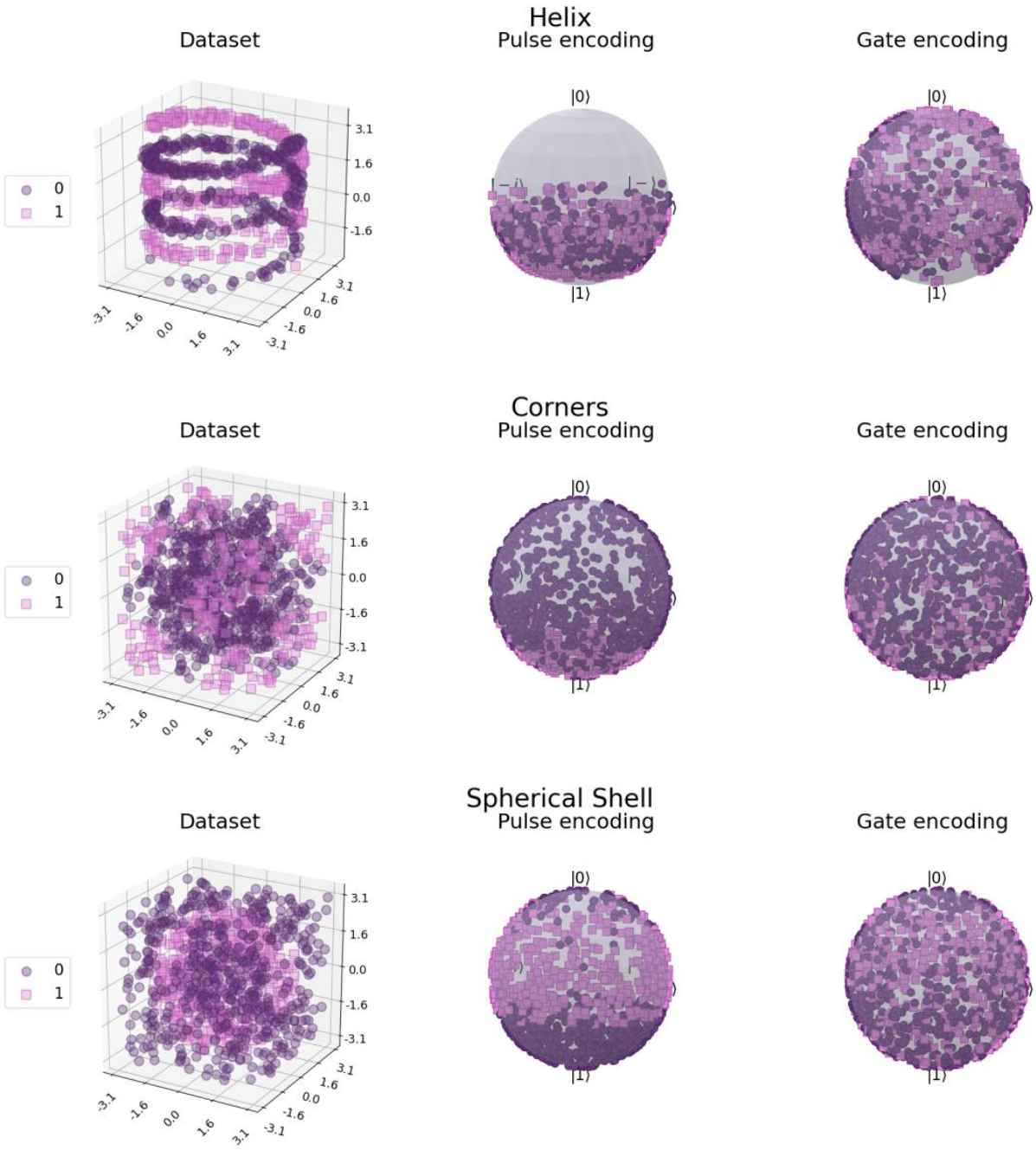

Figure 4: One step encoding applied to **helix, corners and shell** datasets the gate-baesd and pulse-based strategies.

For more general datasets, such as *MNIST Fashion* and *MNIST Digits*, the pulse-based encoding demonstrates its robustness by producing a more organized and interpretable representation on the Bloch sphere. This organized distribution facilitates the separation of classes, although the gate-based method produces results of similar quality. The slight advantage of the pulse-based encoding in terms of interpretability and organization does not translate into significantly better classification performance, indicating that for datasets without explicit geometric structure, the choice of encoding has a reduced impact on overall outcomes. Both methods effectively achieve comparable results, emphasizing the versatility of the pulse-based encoding in handling diverse dataset characteristics.

The *sinus* dataset, however, presents a unique challenge. Neither the pulse-based nor the gate-based encoding is able to produce a discernible organization, likely due to the dataset's lack of inherent geometric structure or alignment with the encodings' assumptions. This further underscores the limitations of both methods when faced with data that does

not lend itself to clear structural interpretation or symmetry.
In general, the pulse-based encoding shows significant promise as a robust method, particularly for datasets with properties conducive to spherical representations or those requiring preservation of the underlying geometric structure. Its ability to leverage the symmetry of such datasets to simplify decision-making boundaries is a clear strength. However, datasets with highly complex or irregular structures, such as the *helix*, reveal its limitations, where alternative encodings like the gate-based method may perform better. This emphasizes the importance of carefully considering dataset characteristics when selecting an encoding strategy, as the optimal choice can vary depending on the data's structural and geometric properties.

3 Main results

The prediction maps generated using a Quantum Neural Network (QNN) with two qubits and two layers were analyzed across all datasets, and the results were compared. These maps, which depict the decision boundaries and model performance, are presented in Figs. 5-10.

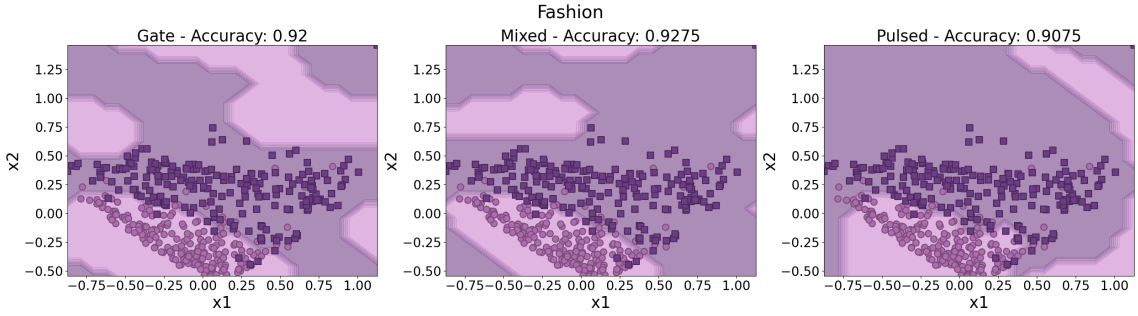

Figure 5: Prediction boundaries for the MNIST **fashion** two-dimensional dataset.

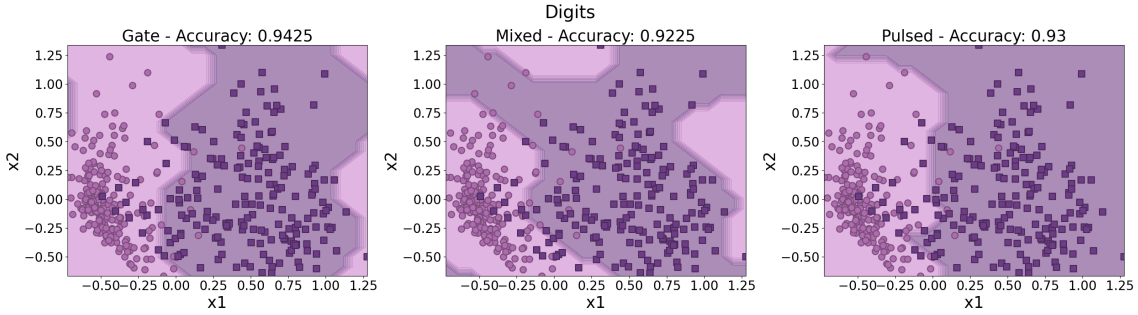

Figure 6: Prediction boundaries for the MNIST **digits** two-dimensional dataset.

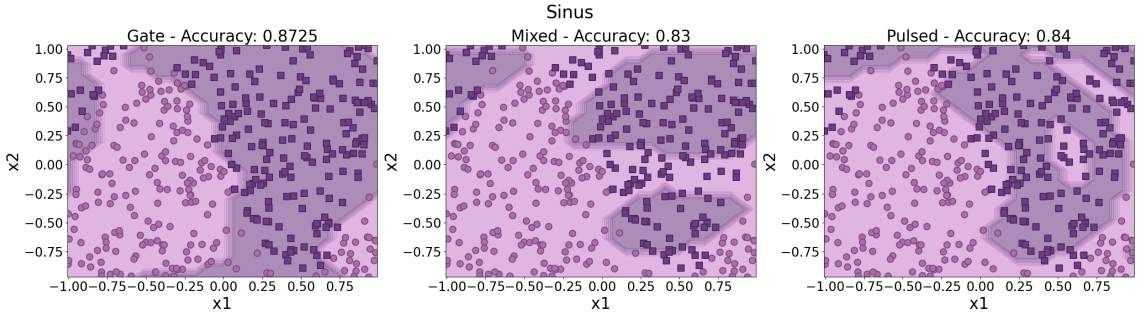

Figure 7: Prediction boundaries for the **sinus** two-dimensional dataset.

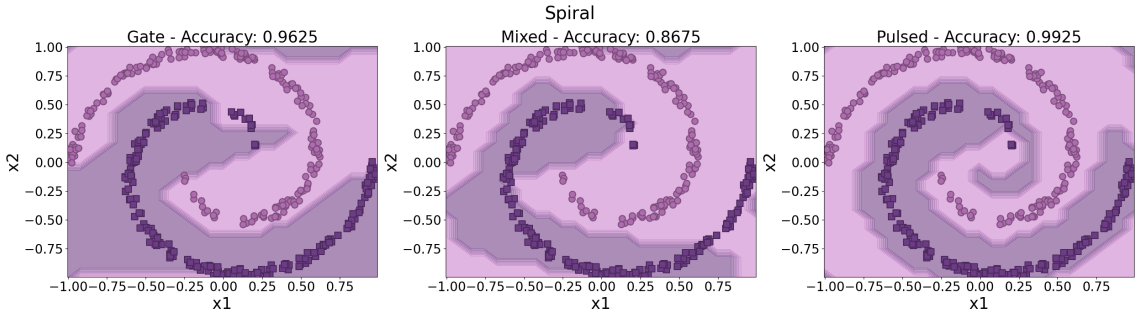

Figure 8: Prediction boundaries for the **spiral** two-dimensional dataset.

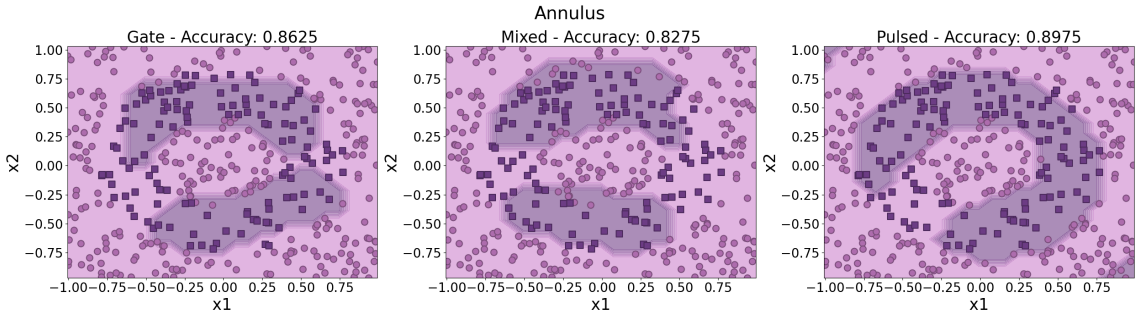

Figure 9: Prediction boundaries for the **annulus** dataset.

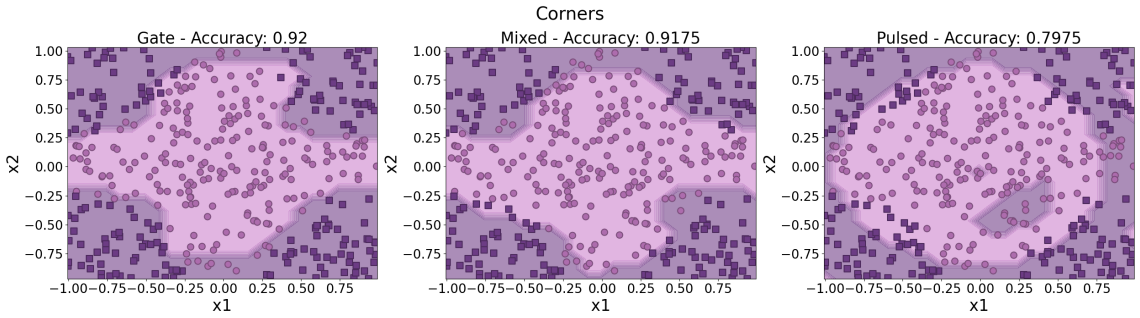

Figure 10: Prediction boundaries for the **corners** two-dimensional dataset.

The mixed and gate-based models yield very similar boundary limits. In contrast, the pulsed model, which incorporates the new pulse encoding strategy, produces distinctly circular boundary limits, as expected from its design. This circular strategy seems advantageous in cases with inherent spherical symmetry, such as the spiral or annulus datasets. However, it may reduce performance in datasets lacking this symmetry. A notable example is the corners dataset, where the pulsed model's circular strategy fails to capture the dataset's structure, leading to a performance drop of approximately 10% compared to models using the original encoding strategy.

For general datasets like MNIST Fashion and MNIST Digits, the boundary limits of the pulsed encoding appear more intuitive—resembling what a human might define. Unlike the other models, the boundaries do not form isolated islands but instead differentiate between two broader class regions.

Overall, the three models achieve similar accuracies, with the pulsed model performing slightly better on average. However, these results are not definitive, as the datasets are two-dimensional while the encodings were designed for three-dimensional data. Nevertheless, these figures provide valuable insights into how each model constructs its decision boundaries.

The main numerical simulations are performed for the six datasets, with the results presented in Figs. **??-??**. A detailed table, which includes the final training loss values, is provided in Table 1.

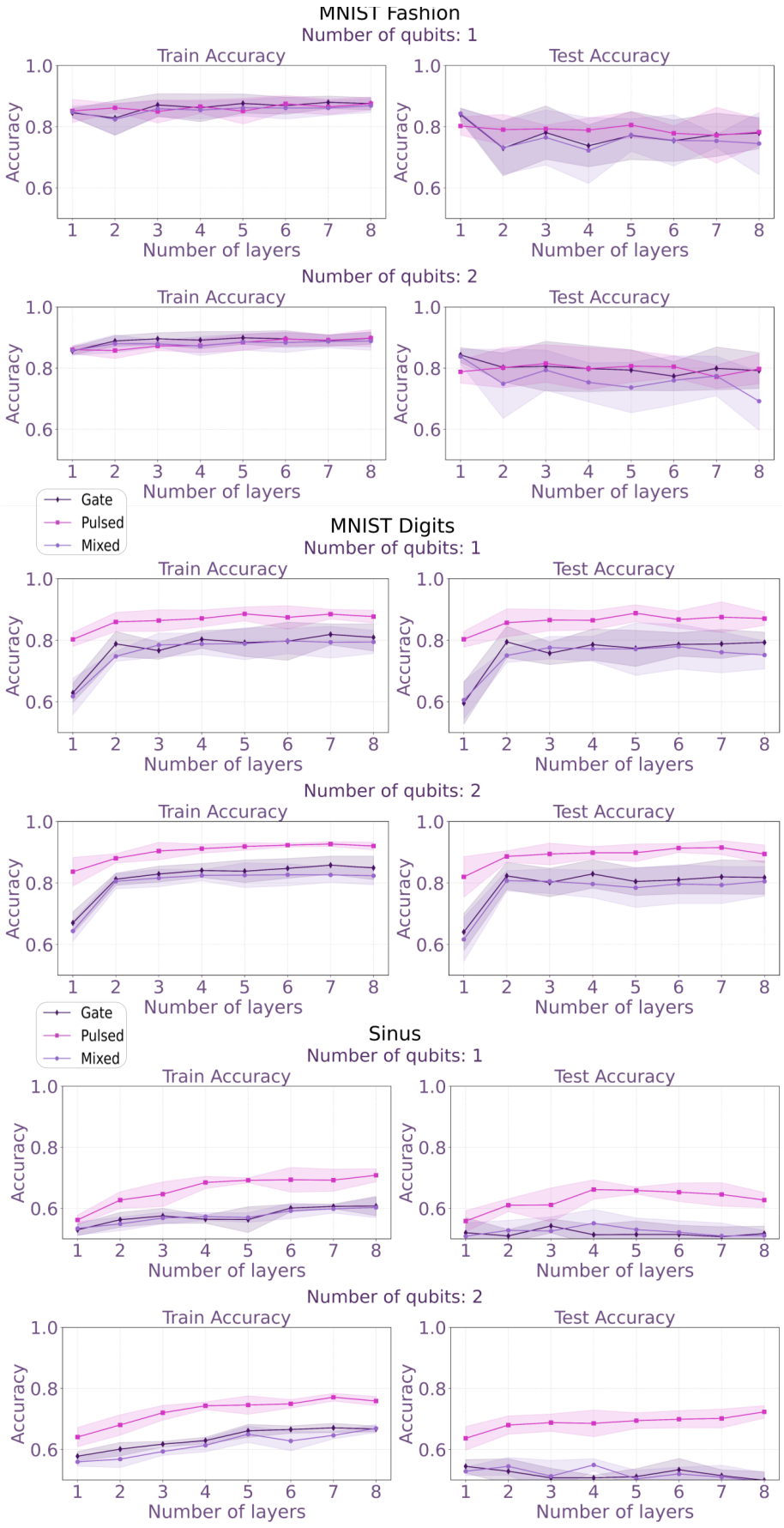

Figure 11: Results for the MNIST and sinus datasets.

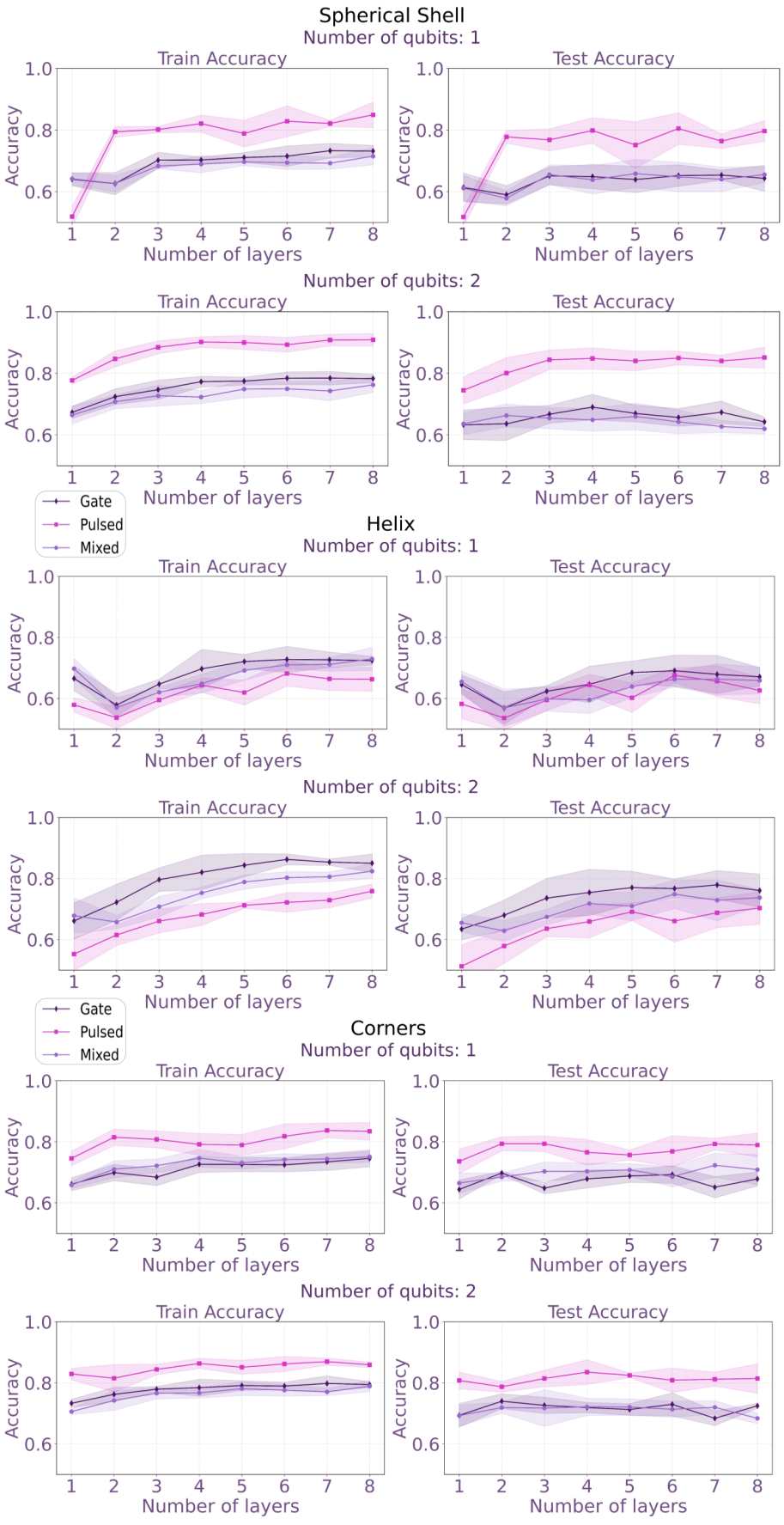

Figure 12: Results for the shell, helix and corners dataset.

As the *MNIST*, *Shell*, and *Sinus* datasets were previously described in the main article, their analysis is omitted here. However, the results for the *Helix* dataset highlight the importance of selecting an appropriate encoding strategy, as it is the only dataset where the PulseQNN yields worse results compared to the original model. In contrast, the *Corners* dataset follows the trend observed in other datasets, with the PulseQNN improving the results. In both cases, the MixedQNN produces results similar to those of the original GateQNN model.

4 Conclusions

The additional results and analysis presented in this supplementary file align with the conclusions of the main article, reinforcing the feasibility of hardware-adapted quantum machine learning. The findings confirm that the proposed new encoding method leads to improved performance in the majority of cases, offering a promising avenue for enhancing QML models. These results highlight the potential of incorporating hardware-specific adaptations into quantum machine learning systems to better exploit the underlying quantum resources.

However, the analysis also underscores the importance of carefully selecting the encoding strategy. While the new encoding generally outperforms traditional methods, there are exceptions, particularly for datasets with complex or unconventional structures. In such cases, alternative encoding strategies may be necessary to ensure optimal model performance. This reinforces the conclusion that, although the new encoding method provides substantial benefits, attention should be paid to the characteristics of the dataset to achieve the best possible results.

In summary, the supplementary analysis not only supports but also elaborates on the main article's conclusion that hardware-adapted QML is a viable and promising approach. It highlights the potential of the new encoding, while also cautioning that the choice of encoding must be carefully tailored to the specific dataset to fully harness the advantages of hardware-adapted quantum models.

A Table results

			Gate			Mixed			Pulsed		
Dataset	**Qubits**	**Layers**	**Train Loss**	**Train Acc**	**Test Acc**	**Train Loss**	**Train Acc**	**Test Acc**	**Train Loss**	**Train Acc**	**Test Acc**
Corners	**1**	1	0.248±0.009	0.66±0.02	0.64±0.03	0.247±0.008	0.66±0.01	0.66±0.03	0.178±0.014	0.75±0.02	0.74±0.04
		2	0.212±0.015	0.70±0.03	0.70±0.01	0.209±0.016	0.71±0.03	0.68±0.01	0.135±0.014	0.81±0.03	0.79±0.02
		3	0.214±0.012	0.68±0.03	0.65±0.02	0.198±0.016	0.72±0.02	0.70±0.03	0.135±0.017	0.81±0.03	0.79±0.03
		4	0.186±0.016	0.73±0.03	0.68±0.03	0.184±0.011	0.75±0.03	0.70±0.03	0.148±0.021	0.79±0.04	0.77±0.04
		5	0.188±0.011	0.73±0.02	0.69±0.02	0.182±0.014	0.73±0.02	0.71±0.02	0.146±0.019	0.79±0.03	0.76±0.02
		6	0.183±0.015	0.72±0.02	0.69±0.03	0.178±0.013	0.74±0.02	0.69±0.03	0.132±0.023	0.82±0.04	0.77±0.05
		7	0.180±0.021	0.73±0.03	0.65±0.03	0.175±0.011	0.74±0.01	0.72±0.04	0.124±0.016	0.84±0.02	0.79±0.02
		8	0.178±0.015	0.75±0.03	0.68±0.02	0.176±0.014	0.75±0.02	0.71±0.05	0.124±0.019	0.83±0.03	0.79±0.04
	2	1	0.173±0.004	0.73±0.01	0.69±0.04	0.191±0.006	0.71±0.01	0.69±0.04	0.129±0.011	0.83±0.02	0.81±0.03
		2	0.158±0.011	0.76±0.02	0.74±0.02	0.170±0.011	0.74±0.03	0.72±0.02	0.127±0.014	0.82±0.05	0.79±0.02
		3	0.154±0.006	0.78±0.01	0.73±0.03	0.161±0.008	0.77±0.02	0.72±0.06	0.118±0.007	0.84±0.02	0.81±0.03
		4	0.147±0.013	0.78±0.03	0.72±0.02	0.157±0.006	0.77±0.02	0.72±0.03	0.105±0.011	0.86±0.02	0.84±0.04
		5	0.147±0.004	0.79±0.02	0.71±0.02	0.158±0.009	0.78±0.02	0.72±0.03	0.109±0.012	0.85±0.02	0.82±0.01
		6	0.144±0.006	0.79±0.01	0.73±0.04	0.158±0.007	0.78±0.02	0.71±0.03	0.107±0.008	0.86±0.02	0.81±0.04
		7	0.143±0.009	0.80±0.03	0.68±0.02	0.159±0.007	0.77±0.01	0.72±0.02	0.102±0.006	0.87±0.01	0.81±0.02
		8	0.142±0.005	0.79±0.01	0.72±0.01	0.154±0.009	0.79±0.02	0.68±0.02	0.104±0.004	0.86±0.01	0.81±0.05
Digits	**1**	1	0.246±0.028	0.63±0.03	0.60±0.07	0.245±0.028	0.62±0.06	0.61±0.06	0.148±0.011	0.80±0.02	0.80±0.03
		2	0.165±0.018	0.79±0.04	0.79±0.05	0.185±0.011	0.75±0.02	0.75±0.02	0.110±0.017	0.86±0.03	0.86±0.05
		3	0.171±0.020	0.77±0.03	0.76±0.04	0.160±0.023	0.78±0.04	0.78±0.04	0.110±0.016	0.86±0.04	0.87±0.03
		4	0.148±0.017	0.80±0.03	0.79±0.05	0.158±0.014	0.79±0.03	0.77±0.04	0.104±0.017	0.87±0.03	0.86±0.03
		5	0.153±0.027	0.79±0.04	0.77±0.06	0.149±0.022	0.79±0.05	0.77±0.09	0.095±0.014	0.89±0.02	0.89±0.03
		6	0.145±0.030	0.80±0.06	0.79±0.04	0.145±0.019	0.80±0.04	0.78±0.07	0.098±0.021	0.87±0.04	0.87±0.03
		7	0.138±0.024	0.82±0.03	0.79±0.05	0.151±0.026	0.79±0.05	0.76±0.07	0.092±0.012	0.88±0.02	0.88±0.05
		8	0.140±0.027	0.81±0.04	0.79±0.03	0.155±0.020	0.79±0.04	0.75±0.05	0.097±0.013	0.88±0.02	0.87±0.02
	2	1	0.215±0.014	0.67±0.04	0.64±0.06	0.225±0.013	0.64±0.03	0.62±0.07	0.119±0.022	0.84±0.05	0.82±0.07
		2	0.144±0.010	0.81±0.02	0.82±0.04	0.150±0.013	0.81±0.02	0.81±0.03	0.097±0.009	0.88±0.01	0.89±0.02
		3	0.132±0.015	0.83±0.03	0.80±0.05	0.143±0.015	0.82±0.03	0.81±0.04	0.088±0.016	0.90±0.03	0.89±0.04
		4	0.123±0.013	0.84±0.02	0.83±0.05	0.137±0.012	0.82±0.02	0.80±0.04	0.079±0.011	0.91±0.01	0.90±0.02
		5	0.124±0.020	0.84±0.04	0.80±0.05	0.134±0.021	0.83±0.04	0.78±0.06	0.070±0.010	0.92±0.01	0.90±0.03
		6	0.119±0.020	0.85±0.03	0.81±0.05	0.130±0.021	0.83±0.04	0.80±0.06	0.074±0.006	0.92±0.01	0.91±0.01
		7	0.114±0.018	0.86±0.03	0.82±0.06	0.132±0.017	0.83±0.02	0.79±0.06	0.070±0.008	0.93±0.01	0.92±0.02
		8	0.120±0.028	0.85±0.04	0.82±0.05	0.134±0.021	0.82±0.03	0.81±0.05	0.073±0.010	0.92±0.01	0.89±0.03
Fashion	**1**	1	0.112±0.010	0.85±0.01	0.84±0.02	0.111±0.010	0.85±0.02	0.84±0.02	0.121±0.017	0.85±0.04	0.80±0.03
		2	0.129±0.037	0.83±0.06	0.73±0.09	0.128±0.031	0.82±0.05	0.73±0.09	0.110±0.007	0.86±0.01	0.79±0.05
		3	0.100±0.025	0.87±0.04	0.78±0.09	0.104±0.017	0.86±0.03	0.76±0.09	0.118±0.024	0.85±0.04	0.79±0.01
		4	0.108±0.026	0.86±0.05	0.74±0.07	0.112±0.023	0.85±0.03	0.72±0.11	0.110±0.023	0.87±0.02	0.79±0.04
		5	0.097±0.023	0.88±0.03	0.77±0.08	0.105±0.016	0.86±0.03	0.77±0.05	0.112±0.024	0.85±0.04	0.81±0.04
		6	0.103±0.021	0.87±0.03	0.75±0.07	0.109±0.021	0.86±0.04	0.76±0.08	0.101±0.016	0.87±0.03	0.78±0.02
		7	0.095±0.014	0.88±0.02	0.77±0.07	0.107±0.017	0.86±0.02	0.75±0.02	0.101±0.015	0.86±0.03	0.77±0.09
		8	0.097±0.014	0.88±0.02	0.78±0.05	0.102±0.016	0.87±0.02	0.74±0.10	0.100±0.013	0.88±0.02	0.78±0.04
	2	1	0.106±0.010	0.86±0.01	0.84±0.02	0.106±0.010	0.86±0.02	0.84±0.02	0.113±0.009	0.86±0.01	0.79±0.04
		2	0.088±0.012	0.89±0.02	0.80±0.05	0.102±0.021	0.88±0.03	0.75±0.11	0.115±0.018	0.86±0.03	0.80±0.07
		3	0.085±0.015	0.90±0.02	0.81±0.08	0.098±0.011	0.88±0.01	0.79±0.07	0.103±0.009	0.87±0.01	0.82±0.06
		4	0.086±0.019	0.89±0.03	0.80±0.07	0.097±0.019	0.87±0.03	0.75±0.06	0.099±0.016	0.87±0.02	0.80±0.07
		5	0.081±0.016	0.90±0.02	0.79±0.07	0.092±0.019	0.89±0.03	0.74±0.08	0.093±0.014	0.88±0.03	0.81±0.05
		6	0.084±0.016	0.90±0.03	0.77±0.05	0.094±0.019	0.88±0.03	0.76±0.08	0.090±0.015	0.90±0.02	0.80±0.04
		7	0.084±0.013	0.89±0.02	0.80±0.07	0.093±0.016	0.89±0.02	0.77±0.06	0.088±0.013	0.89±0.02	0.77±0.04
		8	0.083±0.012	0.90±0.02	0.79±0.06	0.090±0.018	0.89±0.03	0.69±0.10	0.086±0.013	0.90±0.03	0.80±0.05

			Gate			Mixed			Pulsed		
Dataset	**Qubits**	**Layers**	**Train Loss**	**Train Acc**	**Test Acc**	**Train Loss**	**Train Acc**	**Test Acc**	**Train Loss**	**Train Acc**	**Test Acc**
Helix	**1**	1	0.245±0.023	0.67±0.04	0.65±0.03	0.243±0.024	0.70±0.03	0.66±0.04	0.231±0.009	0.58±0.02	0.58±0.05
		2	0.245±0.009	0.58±0.04	0.57±0.05	0.252±0.016	0.57±0.03	0.57±0.06	0.241±0.011	0.54±0.04	0.54±0.04
		3	0.225±0.012	0.65±0.02	0.62±0.02	0.241±0.007	0.62±0.02	0.60±0.04	0.232±0.013	0.60±0.02	0.60±0.03
		4	0.201±0.026	0.70±0.06	0.65±0.06	0.225±0.017	0.65±0.03	0.60±0.04	0.223±0.017	0.64±0.02	0.64±0.03
		5	0.193±0.011	0.72±0.02	0.68±0.04	0.206±0.010	0.69±0.03	0.64±0.04	0.223±0.016	0.62±0.04	0.60±0.05
		6	0.189±0.021	0.73±0.04	0.69±0.05	0.195±0.005	0.71±0.01	0.66±0.03	0.208±0.018	0.68±0.04	0.68±0.02
		7	0.183±0.010	0.73±0.03	0.68±0.06	0.195±0.013	0.71±0.02	0.66±0.05	0.208±0.011	0.66±0.04	0.66±0.05
		8	0.183±0.009	0.72±0.01	0.67±0.03	0.184±0.015	0.73±0.04	0.66±0.04	0.205±0.015	0.66±0.04	0.63±0.04
	2	1	0.229±0.016	0.66±0.06	0.63±0.04	0.234±0.020	0.68±0.06	0.66±0.03	0.238±0.009	0.55±0.05	0.51±0.07
		2	0.192±0.018	0.72±0.06	0.68±0.05	0.212±0.012	0.66±0.02	0.63±0.03	0.224±0.007	0.62±0.03	0.58±0.06
		3	0.162±0.013	0.80±0.04	0.74±0.06	0.192±0.011	0.71±0.03	0.67±0.02	0.206±0.007	0.66±0.04	0.64±0.03
		4	0.142±0.022	0.82±0.06	0.75±0.08	0.176±0.004	0.75±0.02	0.72±0.03	0.194±0.004	0.68±0.04	0.66±0.05
		5	0.130±0.013	0.84±0.04	0.77±0.05	0.158±0.010	0.79±0.02	0.71±0.05	0.184±0.003	0.71±0.01	0.69±0.03
		6	0.119±0.011	0.86±0.02	0.77±0.03	0.153±0.009	0.80±0.02	0.75±0.05	0.178±0.005	0.72±0.03	0.66±0.07
		7	0.117±0.005	0.85±0.01	0.78±0.05	0.144±0.006	0.81±0.02	0.73±0.07	0.179±0.010	0.73±0.02	0.69±0.05
		8	0.121±0.012	0.85±0.03	0.76±0.05	0.139±0.006	0.82±0.02	0.74±0.03	0.171±0.005	0.76±0.02	0.70±0.05
Shell	**1**	1	0.253±0.010	0.64±0.02	0.61±0.05	0.252±0.009	0.64±0.02	0.61±0.04	0.290±0.006	0.52±0.03	0.52±0.03
		2	0.242±0.022	0.63±0.04	0.59±0.03	0.242±0.013	0.63±0.03	0.58±0.02	0.157±0.009	0.79±0.02	0.78±0.02
		3	0.205±0.016	0.70±0.03	0.65±0.03	0.213±0.012	0.68±0.01	0.66±0.03	0.147±0.011	0.80±0.01	0.77±0.04
		4	0.200±0.012	0.70±0.01	0.65±0.04	0.213±0.012	0.69±0.03	0.64±0.05	0.133±0.007	0.82±0.03	0.80±0.04
		5	0.200±0.006	0.71±0.02	0.64±0.04	0.205±0.007	0.70±0.01	0.66±0.05	0.144±0.018	0.79±0.04	0.75±0.08
		6	0.193±0.020	0.72±0.03	0.65±0.03	0.209±0.013	0.69±0.02	0.65±0.05	0.130±0.015	0.83±0.05	0.80±0.05
		7	0.181±0.014	0.73±0.02	0.65±0.02	0.203±0.014	0.69±0.02	0.64±0.04	0.134±0.006	0.82±0.01	0.76±0.02
		8	0.184±0.006	0.73±0.02	0.64±0.04	0.193±0.013	0.71±0.03	0.66±0.03	0.121±0.017	0.85±0.04	0.80±0.03
	2	1	0.209±0.007	0.67±0.02	0.63±0.05	0.217±0.009	0.66±0.03	0.64±0.03	0.161±0.004	0.78±0.01	0.74±0.04
		2	0.187±0.009	0.72±0.03	0.64±0.05	0.194±0.009	0.71±0.02	0.66±0.04	0.131±0.009	0.85±0.03	0.80±0.05
		3	0.170±0.013	0.75±0.03	0.67±0.03	0.185±0.015	0.73±0.03	0.65±0.03	0.112±0.011	0.88±0.02	0.84±0.03
		4	0.163±0.008	0.77±0.02	0.69±0.04	0.182±0.012	0.72±0.02	0.65±0.04	0.103±0.012	0.90±0.02	0.85±0.03
		5	0.158±0.008	0.77±0.01	0.67±0.03	0.174±0.009	0.75±0.03	0.66±0.04	0.100±0.010	0.90±0.02	0.84±0.03
		6	0.155±0.013	0.78±0.02	0.66±0.03	0.176±0.008	0.75±0.02	0.64±0.04	0.104±0.007	0.89±0.02	0.85±0.02
		7	0.154±0.006	0.78±0.02	0.67±0.04	0.176±0.012	0.74±0.03	0.63±0.02	0.099±0.009	0.91±0.02	0.84±0.02
		8	0.154±0.008	0.78±0.01	0.64±0.02	0.165±0.011	0.76±0.02	0.62±0.02	0.091±0.005	0.91±0.02	0.85±0.03
Sinus	**1**	1	0.297±0.009	0.53±0.02	0.52±0.05	0.297±0.010	0.53±0.02	0.51±0.04	0.271±0.009	0.56±0.02	0.56±0.03
		2	0.276±0.008	0.56±0.02	0.51±0.02	0.285±0.009	0.55±0.02	0.53±0.03	0.234±0.011	0.63±0.03	0.61±0.02
		3	0.273±0.007	0.58±0.02	0.54±0.02	0.279±0.012	0.57±0.02	0.53±0.05	0.221±0.016	0.65±0.04	0.61±0.06
		4	0.266±0.003	0.56±0.01	0.51±0.03	0.265±0.008	0.57±0.01	0.55±0.05	0.207±0.010	0.68±0.02	0.66±0.03
		5	0.269±0.015	0.56±0.04	0.51±0.04	0.272±0.002	0.57±0.02	0.53±0.04	0.211±0.003	0.69±0.01	0.66±0.01
		6	0.252±0.010	0.60±0.01	0.51±0.03	0.263±0.007	0.59±0.03	0.52±0.04	0.204±0.011	0.69±0.04	0.65±0.03
		7	0.253±0.009	0.61±0.01	0.51±0.03	0.262±0.004	0.60±0.01	0.51±0.04	0.202±0.013	0.69±0.04	0.65±0.04
		8	0.251±0.010	0.61±0.03	0.52±0.02	0.256±0.008	0.60±0.03	0.51±0.02	0.194±0.012	0.71±0.02	0.63±0.02
	2	1	0.243±0.001	0.58±0.02	0.54±0.02	0.253±0.009	0.56±0.01	0.53±0.01	0.221±0.005	0.64±0.03	0.64±0.04
		2	0.239±0.006	0.60±0.02	0.53±0.04	0.251±0.013	0.57±0.03	0.54±0.03	0.201±0.007	0.68±0.03	0.68±0.03
		3	0.231±0.004	0.62±0.01	0.51±0.03	0.241±0.006	0.59±0.01	0.51±0.05	0.188±0.011	0.72±0.02	0.69±0.03
		4	0.226±0.007	0.63±0.01	0.51±0.01	0.237±0.006	0.61±0.02	0.55±0.02	0.179±0.010	0.74±0.01	0.69±0.04
		5	0.218±0.012	0.66±0.02	0.51±0.03	0.226±0.009	0.65±0.03	0.50±0.03	0.175±0.011	0.75±0.03	0.69±0.03
		6	0.214±0.007	0.67±0.01	0.53±0.04	0.229±0.007	0.63±0.03	0.52±0.02	0.170±0.007	0.75±0.01	0.70±0.03
		7	0.210±0.007	0.67±0.01	0.51±0.02	0.221±0.004	0.65±0.01	0.51±0.04	0.164±0.008	0.77±0.01	0.70±0.03
		8	0.212±0.007	0.67±0.01	0.50±0.03	0.215±0.005	0.67±0.01	0.50±0.03	0.165±0.009	0.76±0.01	0.72±0.02

Table 1: Results for different datasets. The values represent the mean of the loss function, training accuracy, and test accuracy, along with their corresponding standard deviations, averaged over five independent runs.

References

[1] P. Rodriguez-Grasa et al. "Training embedding quantum kernels with data re-uploading quantum neural networks". arXiv:2401.04642 (2024).